Cancer Letters 605 (2024) 217265

Contents lists available at ScienceDirect

Cancer Letters

journal homepage: www.elsevier.com/locate/canlet

Original Articles

# Integration of transcriptomics, proteomics and loss-of-function screening reveals WEE1 as a target for combination with dasatinib against proneural glioblastoma

Obada T. Alhalabi [a,b,1], Mona Göttmann [a,1], Maxwell P. Gold [c,1], Silja Schlue [a], Thomas Hielscher [d], Murat Iskar [e], Tobias Kessler [f,g], Ling Hai [g], Tolga Lokumcu [a], Clara C. Cousins [c], Christel Herold-Mende [h], Bernd Heßling [i], Sandra Horschitz [j,k,l], Ammar Jabali [j,k,l], Philipp Koch [j,k,l], Ulrich Baumgartner [m,n], Bryan W. Day [m,n], Wolfgang Wick [f,g], Felix Sahm [o], Sandro M. Krieg [b], Ernest Fraenkel [c,p], Emma Phillips [a], Violaine Goidts [a,*]

[a] Brain Tumor Translational Targets, DKFZ Junior Group, German Cancer Research Center (DKFZ), Heidelberg, Germany
[b] Department of Neurosurgery, University Hospital Heidelberg, Heidelberg, Germany
[c] Department of Biological Engineering, Massachusetts Institute of Technology (MIT), Cambridge, MA, USA
[d] Division of Biostatistics (C060), German Cancer Research Center, Germany
[e] Division of Molecular Genetics, Heidelberg Center for Personalized Oncology, German Cancer Research Consortium (DKTK), German Cancer Research Center (DKFZ), Heidelberg, Germany
[f] Clinical Cooperation Unit Neurooncology, German Cancer Research Center (DKFZ), Heidelberg, Germany
[g] Department of Neurology and Neurooncology Program, National Center for Tumor Diseases, Heidelberg University Hospital, Heidelberg, Germany
[h] Division of Experimental Neurosurgery, Department of Neurosurgery, Heidelberg University Hospital, 69120, Heidelberg, Germany
[i] Genomics and Proteomics Core Facility, German Cancer Research Center (DKFZ), Heidelberg, Germany
[j] Central Institute of Mental Health, University of Heidelberg/Medical Faculty Mannheim, Mannheim, Germany
[k] Hector Institute for Translational Brain Research (HITBR gGmbH), Mannheim, Germany
[l] German Cancer Research Center (DKFZ), Heidelberg, Germany
[m] Cell and Molecular Biology Department, QIMR Berghofer Medical Research Institute, Sid Faithfull Brain Cancer Laboratory, Brisbane, QLD, 4006, Australia
[n] School of Biomedical Sciences, The University of Queensland, Brisbane, 4072, Australia
[o] Department of Neuropathology, Institute of Pathology, University Hospital Heidelberg, Heidelberg, Germany
[p] Eli and Edythe Broad Institute of MIT and Harvard, Cambridge, MA, USA

## ARTICLE INFO

*Keywords:*
Phosphoproteomics
Computational integration
Loss-of-function shRNA screen
Dasatinib
WEE1

## ABSTRACT

Glioblastoma is characterized by a pronounced resistance to therapy with dismal prognosis. Transcriptomics classify glioblastoma into proneural (PN), mesenchymal (MES) and classical (CL) subtypes that show differential resistance to targeted therapies. The aim of this study was to provide a viable approach for identifying combination therapies in glioblastoma subtypes. Proteomics and phosphoproteomics were performed on dasatinib inhibited glioblastoma stem cells (GSCs) and complemented by an shRNA loss-of-function screen to identify genes whose knockdown sensitizes GSCs to dasatinib. Proteomics and screen data were computationally integrated with transcriptomic data using the SamNet 2.0 algorithm for network flow learning to reveal potential combination therapies in PN GSCs. *In vitro* viability assays and tumor spheroid models were used to verify the synergy of identified therapy. Further *in vitro* and TCGA RNA-Seq data analyses were utilized to provide a mechanistic explanation of these effects. Integration of data revealed the cell cycle protein WEE1 as a potential combination therapy target for PN GSCs. Validation experiments showed a robust synergistic effect through combination of dasatinib and the WEE1 inhibitor, MK-1775, in PN GSCs. Combined inhibition using dasatinib and MK-1775 propagated DNA damage in PN GCSs, with GCSs showing a differential subtype-driven pattern of expression of cell cycle genes in TCGA RNA-Seq data. The integration of proteomics, loss-of-function screens and transcriptomics confirmed WEE1 as a target for combination with dasatinib against PN GSCs. Utilizing this

* Corresponding author. Brain Tumor Translational Targets, German Cancer Research Center (DKFZ), 69120, Heidelberg, Germany.
*E-mail address:* v.goidts@dkfz.de (V. Goidts).
[1] Authors share first authorship.

https://doi.org/10.1016/j.canlet.2024.217265
Received 24 July 2024; Received in revised form 17 September 2024; Accepted 18 September 2024
Available online 25 September 2024

integrative approach could be of interest for studying resistance mechanisms and revealing combination therapy targets in further tumor entities.

## 1. Introduction

Glioblastoma (GB) is the most common malignancy of the nervous system [1]. Even under maximal surgical resection, adjuvant radiation and chemotherapy, patients show an overall median survival around 15 months after diagnosis [2]. Genomic, methylomic, transcriptomic, and proteomic studies have revealed molecular heterogeneity between and within GB samples [3,4] yielding, amongst others, a classification system including three RNA-based subtypes: the mesenchymal (MES), proneural (PN), and classical (CL) [5]. Single-cell and lineage-tracing studies have underlined the exceptional heterogeneity GB exhibits, showing a spatial and temporal diversity of subtypes even within the same patient [6,7]. Further studies have also highlighted a sub-population of cells termed GB stem-like cells (GSCs), which are implicated in resistance to chemo-radiotherapy because they can remain dormant and re-establish tumor growth after treatment is complete [8–10].

In a previous study, we showed that MES GSCs were more sensitive to tyrosine-kinase inhibitor dasatinib than PN GSCs [11]. However, a combination therapy capable of eradicating both MES and PN GSCs would be more effective against such a heterogeneous disease. In this work, we hence used two experimental approaches to study dasatinib response and identify potential combination therapies to improve efficacy against PN cells. First, we generated protein and phosphoprotein data from treated and untreated GSCs of the MES and PN subtype to better comprehend the possible subtype-driven molecular response to dasatinib therapy. Next, we applied a pooled shRNA drop-out screen to dasatinib-treated MES and PN GSCs. Indeed, shRNA screens have been previously used to study tumor vulnerability in other cancers [12–14]. In such drop-out screens, the effect of an shRNA-induced gene knockdown on cell viability is determined. If the knockdown of a particular gene causes depletion of the transduced cells (i. e. they drop out of the screen), the gene can be considered essential for GSC viability under these conditions. In this study, we performed screens including dasatinib and vehicle treated GSCs from both subtypes to identify genes contributing to dasatinib resistance, particularly in PN GSCs.

We also sought to computationally integrate the hits from both assays to more comprehensively understand the subtype-specific dasatinib response. Network flow algorithms such as ResponseNet [15] and SamNet [16] have been previously used to integrate data from multiple biological assays. These methods work by creating a directed network with hits from one assay (e. g. proteomics) at the top and from another assay (e. g. shRNA screen) at the bottom. These hits are connected through a protein-protein interaction network where edges represent physical protein-protein interactions (PPI). Flow travels from the top of the network, through some selected proteins from the PPI, down to the bottom, resulting in a subnetwork of particularly important proteins that connect the two datasets. These methods have led to biological insights about Parkinson's disease [15] and lung cancer [16] but are limited because they do not adjust for high-degree hub nodes and cannot handle hits from more than two biological assays.

In this work, we modified the SamNet algorithm (i. e. SamNet 2.0) to address these limitations and integrate the proteomics response data with the shRNA screen hits. Specifically, we implemented SamNet 2.0 to incorporate baseline RNA expression and reduce hub node bias in the network flow pattern. Such improvements are critical when not all genes or proteins in the true network may be evaluated experimentally. Analysis of the individual assays and integrated network highlighted cell cycle genes and specifically WEE1 as an attractive target for combination therapy in PN cells. This hypothesis was validated and mechanistically described in cell line and tumor-bearing cerebral spheroid models, and further consolidated using GB patient data, suggesting that WEE1 inhibition in addition to dasatinib could be an effective combination for eliminating cells of the MES and PN subtypes in GB.

## 2. Methods

### 2.1. SILAC (stable isotope labeling of amino acids in cell culture) with mass spectrometry

NCH711d and NCH705 (MES) and NCH421k and NCH644 (PN) were cultured with SILAC heavy and light medium (DMEM:F12 with Arg-10 and Lys-6) for 6 doublings. After that, cell pellets were isolated, and protein extracted according to the phosphoprotein isolation protocol (see below) for incorporation percentage check. After confirming 95 % incorporation in 'heavy' samples, GSCs containing 'heavy' amino acids were treated with 1 μM dasatinib and 'light' GSCs with DMSO vehicle control for 72 h 1 million cells were isolated for the day-4 time point. The remaining GCSs were further cultured under the same conditions and further reseeded and retreated with the same dasatinib concentration on day 8 and cultured for a further four days, totaling 12 days of inhibition. GSC pellets were then harvested, and proteins isolated for proteomics and phosphoproteomics.

### 2.2. Proteomics and phosphoproteomics differential analysis

The proteomics and phosphoproteomics data were filtered down to features present in all samples. Additionally, for the proteomics data, features were only included if they mapped to a single protein. Ensembl BioMart [17] was used to account for gene synonyms output by MaxQuant. In the case where a feature mapped to two proteins, but the first protein product is a part of the second protein product as well (e. g. ARPC4 and the ARPC4-TTLL3 readthrough protein), this was considered as uniquely mapping to the first protein. For the phosphoproteomics data, phosphosites were named according to their amino acid motif ( ± 7 AA from the phosphosite); multiple instances containing the same AA motif were collapsed to a single value by taking the mean. Limma was used for all differential analyses on the log2-normalized quantification values for the proteins and phosphosites. The Benjamini-Hochberg method was used to adjust for multiple hypotheses.

### 2.3. Phosphosite set analysis

PTM-SEA [18] was run on the results from the limma analysis of the phosphosite data, using the amino acid motifs ( ± 7 amino acids from the phosphosite) and the flanking sequence human dataset (v.1.9.0) from PTMSigDB [18]. There were three values tested: 1) the change in response in MES GSCs (i.e. limma t-value from one-sample *t*-test of only MES GSCs), 2) the change in response in PN GSCs (i.e. limma t-value from one-sample *t*-test of only PN GSCs), and 3) the difference in response between MES and PN GCSs (limma t-value from *t*-test between MES vs. PN). The t-statistic was used instead of a p-value because PTM-SEA considers directionality of trends. PTM-SEA was run with the standard parameters, except the minimum set overlap was reduced from 10 to 5 because of the limited number of phosphosite-sets being considered with the standard implementation. For further information on kinase identification please refer to supplementary methods.

### 2.4. TCGA RNA-Seq samples analysis

The gene expression data [log2(FPKM + 1)] of 230 IDH wildtype glioblastoma samples were obtained from UCSC Xena (http://xena.ucsc.

edu). In boxplots, the comparison p-values of gene expression levels between molecular subtypes were performed by the Mann-Whitney test using ggpubr (v.0.4.0). ns: $p > 0.05$, *: $p \leq 0.05$, **: $p \leq 0.01$, ***: $p \leq 0.001$, ****: $p \leq 0.0001$. In heatmaps, the gene expression levels of cell cycle signatures were scaled and centered by the scale function, and then clustered by the k-means clustering using ComplexHeatmap (v.2.6.2).

### 2.5. Cellecta® DECIPHER® pooled drop-out loss-of-function screen

GSCs (NCH711d, NCH705, NCH421k and NCH644) were transduced with a target MOI (multiplicity of infection) of 0.5 with the lentiviral constructs containing module 1 of the DECIPHER library from Cellecta®. Half of the transduced GSCs were harvested at 18 h post-transduction as a baseline sample. 24 h after transduction, the medium was changed. 72 h after transduction, flow cytometry was used to verify correct transduction percentage and confirm the desired MOI. Transduced GSCS were then split into two arms: one was treated with the respective $IC_{20}$ concentration of dasatinib, the other with the corresponding DMSO dilution. GCSs were further cultured until reaching 8–10 doublings by splitting every 4 days with dasatinib/DMSO reapplied to the respective culture and the TagRFP-positivity monitored. After reaching the desired doubling number, final pellets of the dasatinib and DMSO arms were harvested for sequencing.

### 2.6. Data analysis of shRNA DECIPHER screen

Endpoint missing values of shRNAs were treated as zero counts. Trimmed mean of M values (TMM) normalization was applied. Unspecific filtering was done prior to testing, keeping only shRNAs with more than 2 counts per million (CPM) in all baseline samples.

To analyze shRNAs for enrichment or depletion, an RNAseq analysis with edgeR (with a negative binomial model) was used [19]. Endpoint missing values of shRNAs were treated as zero counts. Significance testing was carried out on both an shRNA- and gene-level for the endpoint compared to baseline. Each gene was tested based on the shRNAs in a gene-set test approach [20]. Genes with a consistent signal across their corresponding shRNAs should therefore be ranked high. In addition to comparing PN and MES separately for enriched and depleted shRNAs under dasatinib and DMSO, samples were tested for shRNAs/-genes that show a significant difference at endpoint between PN and MES, all compared to the baseline, i.e., modelling an interaction effect between type and treatment and accounting for the sample effect. For visualization, shRNA counts were normalized with results expressed as log-transformed counts per Million (CPM).

### 2.7. Implementation of SamNet 2.0

SamNet 2.0 was implemented to gain a better understanding of the subtype-specific effects of dasatinib on glioblastoma cell lines. The SamNet 2.0 graph was designed such that proteomic hits received inputs from the source and shRNA hits had outgoing edges into the terminal sink node. Proteomics hits for each subtype were proteins significantly affected by dasatinib (i. e. one-sample *t*-test was significantly different from 0), with an absolute mean $\log_2$FC greater than 1. The shRNA hits were selected on two criteria: 1) knockdown of this gene caused significantly different ($p < 0.01$) survival effects between the dasatinib-treated cells and the DMSO treated cells 2) the $\log_2$FC in survival between the dasatinib-treated cells and the untreated cells is more extreme than 1 in the same direction as the DMSO comparison. Please refer to supplementary methods for further information on threshold values.

### 2.8. Generation of human cerebral spheroids

Cerebral spheroids were generated as previously described [21]. Briefly, neural precursor cells (NPCs) were derived from human induced pluripotent stem cells (hiPSCs) by dual inhibition of SMAD signaling in medium composed of advanced DMEM/F12 (Thermo Fisher Scientific), B27 (1 %; Thermo Fisher Scientific), GlutaMax (1 %; Thermo Fisher Scientific), Pen/Strep (1 %; Thermo Fisher Scientific), and the small molecules LDN-193189 (1 μM; Miltenyi Biotech), XAV (2 μM; Cell Guidance Systems) and SB-431542 (10 μM; Cell Guidance Systems). After 8 days the concentration of LDN-193189 was reduced to 200 nM and SB-431542 was omitted. NPCs were dissociated into single cells using TrypLE Express and plated in a U-bottom shaped 96 well-plate precoated with 0.5 % Pluronic (100000 cells/well) in the same medium (without small molecules) supplemented with 50 μM ROCK inhibitor Y-27632 (Cell Guidance Systems). Two days later, aggregates were transferred into 6 cm-dishes precoated with 0.5 % Pluronic and medium was changed to DMEM/F12, 1 % B27, 1 % GlutaMax, 1 % P/S, and non-essential amino acids (1 %; Thermo Fisher Scientific) supplemented with EGF and FGF-2 (both 20 ng/ml; Cell Guidance Systems) for the next 19 days with medium changes every other day. After this expansion phase, the growth factors FGF-2 and EGF were omitted from the medium and neuronal differentiation was promoted by inhibition of Notch signaling as previously described [22].

Due to suppression of the generation of mesodermal and endodermal germ layers via dual inhibition of SMAD signaling using SB-431542 and LDN193189 we facilitate the generation of neuroectoderm. Thereby, the cell types in our spheroids at the time of coculture with tumor cells are limited to neurons and astrocytes [23].

### 2.9. Co-culture of Glioblastoma cells expressing luciferase and GFP with cerebral spheroids

To establish NCH644 cells stably co-expressing luciferase and GFP, NCH644 were transduced with pGF1 virus and subsequently sorted for $GFP^+$-cells using the BD FACS Aria Fusion-3 prior to starting the co-culture experiment. Spheroids were cultured in advanced MEM (Thermo Fisher Scientific), B27 (1:100), GlutaMax (1 %), Glucose (5 mg/ml), Pen/Strep (1 %) 7 days prior to the coculture start. The tumor cell culture (luciferase and GFP-expressing NCH644 GSC line) was dissociated into single cells using accutase and 7500 tumor cells were plated together with one spheroid per well of a U-bottom shaped 96 well-plate precoated with 0.5 % Pluronic in the same medium supplemented with EGF and FGF (20 ng/ml each). After two days, spheroids were transferred into a cell culture dish precoated with 0.5 % Pluronic. Medium was changed every other day. After 7 days of coculture, the growth factors EGF and FGF were withdrawn and tumor-cell-infiltrated spheroids were further cultured until day 13. On day 14, drug exposure to 0.75 μM MK-1775 or 5 μM Dasatinib as single or combinatorial treatment was started in parallel to a respective DMSO control. Tumor growth was assessed via luminescence measurements at 4-, 8- and 12-days post-treatment, in addition to apoptosis and cell proliferation at day 12. For each treatment condition, 6 spheroids were used to cover cerebral spheroid heterogeneity and invasion capacity.

### 2.10. Measuring of bioluminescence of spheroid co-culture

Bioluminescent signals were measured before treatment start, followed by measurements every 4 days. For quantification of tumor growth in the spheroid co-culture experiment, bioluminescent signal was measured using the IVIS® Lumina LT Series III (PerkinElmer). Before signal acquisition, spheroid co-cultures were incubated with 150 μg/ml D-luciferin for 30 min at RT. Using a black-walled 96-well plate, the bioluminescent signal was acquired with an integration time of 15 s and total flux per defined region was quantified using the Living Image® software.

### 2.11. Cell cycle analysis

To study cell cycle phases upon treatment with dasatinib and MK-

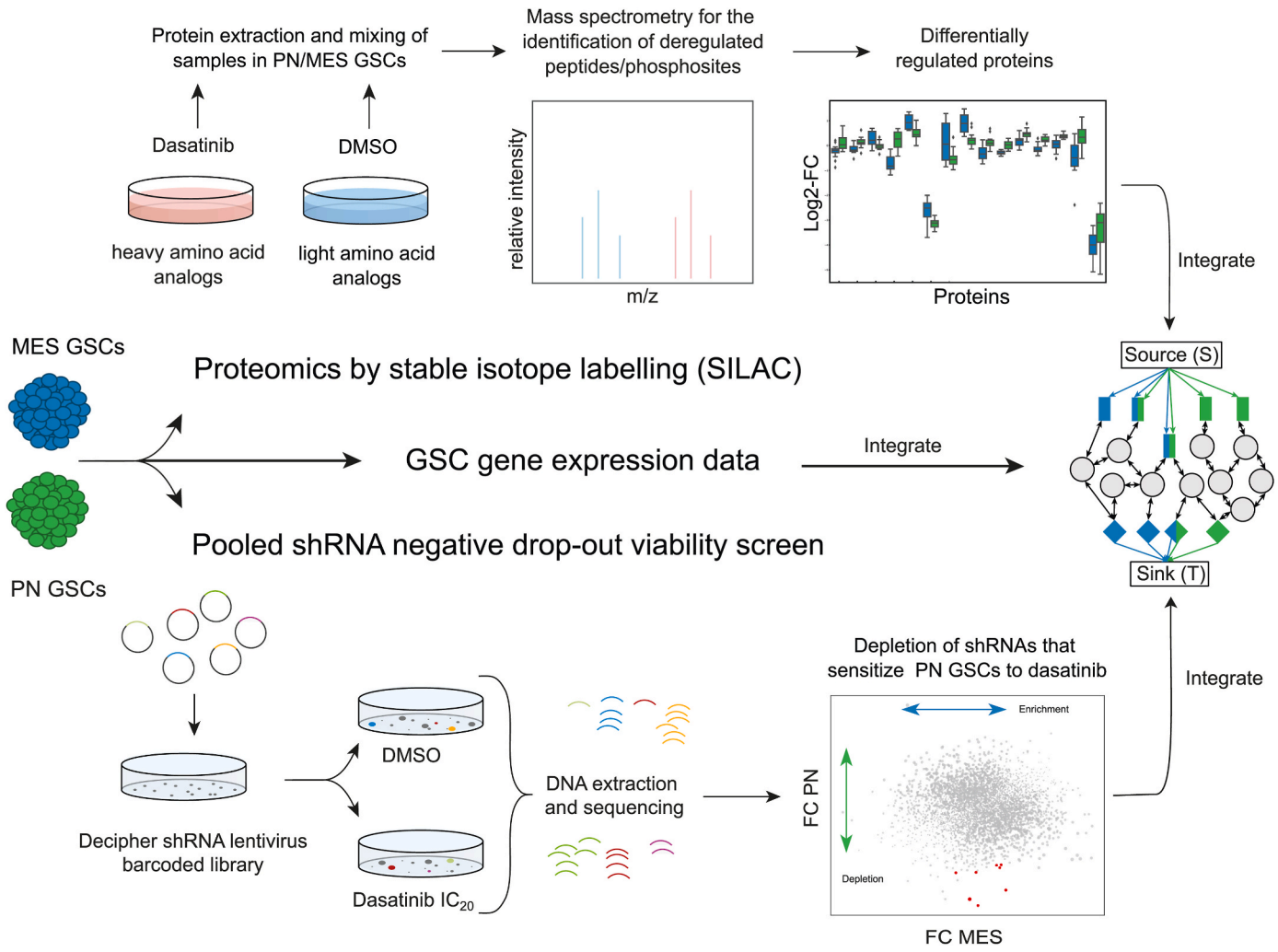


**Fig. 1.** Integrated multi-omics approach to tackle resistance to dasatinib in proneural Glioblastoma stem-like cells (PN GCSs). After stable isotope labeling with amino acids in cell culture (SILAC) and subsequent inhibition with dasatinib, PN and MES GSCs underwent phosphoproteomic analyses using mass spectrometry to study intracellular signal transduction pathways that are deregulated upon dasatinib treatment (upper part). This was complemented by a functional drop-out viability screen using a pooled barcoded shRNA library against 5000 human genes combined with dasatinib. This screen exposed several genes whose knock-down increased sensitivity to dasatinib inhibition and provided targets for combinatory drug inhibition (lower part). Both screen outputs were then integrated using SamNet 2.0, which also factored in gene expression data (middle part) to reveal possible combination therapy targets. MES = mesenchymal. DMSO = dimethyl sulfoxide. FC = fold-change. m/z = mass to charge ratio. $IC_{20}$ = inhibition concentration at which 80 % of inhibited cells show viability.

1775 in NCH cell lines, propidium iodide staining was conducted followed by FACS analysis. 100 000 cells/mL were seeded in a 12-well assay plates and treated with single or double treatment of 5 μM dasatinib, 0.75 μM MK-1775 and the respective controls. 24 and 48 h post-treatment, cells were collected, washed with PBS and dissociated using Accutase®. After centrifugation, cells were washed with PBS prior to resuspension in 500 μL PBS. To fix cells, 1.2 mL precooled 70 % ethanol solution was added drop-wise to the singularized cells while vortexing. Cells were fixed at −20 °C overnight, then centrifuged for 10 min at 2000 rpm. After a washing step in 1 % BSA in PBS, cells were resuspended and incubated for 20 min in 500 μL 0.25 % Triton X-100 in PBS. Followed by a centrifugation step of 5 min at 2000 rpm, cells were resuspended in 150 μL PI-staining solution (0.1 % Triton X-100 in PBS supplemented with 50 μg/mL PI and 200 μg/mL RNAseA) and incubated for 10 min at 37 °C and 10 min at RT before acquisition. Cell cycle phases were analyzed using a LSRFortessa and quantified with FACS-Diva Software.

## 3. Results

### 3.1. Integration of proteomics and loss-of-function screen to overcome dasatinib resistance in PN GSCs

To reveal the differential response to inhibition in PN and MES GSCs on a proteomic and phosphoproteomic level, SILAC (stable isotope labelling in cell culture) with mass spectrometry was implemented in dasatinib treated GSCs. This was complimented by functional genomics, using a pooled shRNA drop-out loss-of-function screen targeting around 5000 genes involved in cell signaling and cancer under simultaneous dasatinib inhibition. To prioritize shRNA screen hits for further validation, we developed and implemented a significantly improved version of the SamNet algorithm (named SamNet 2.0). This method allowed for the integration of shRNA screen hits and proteomic response data, while also considering the baseline gene expression levels of each gene for each cell type (Fig. 1).

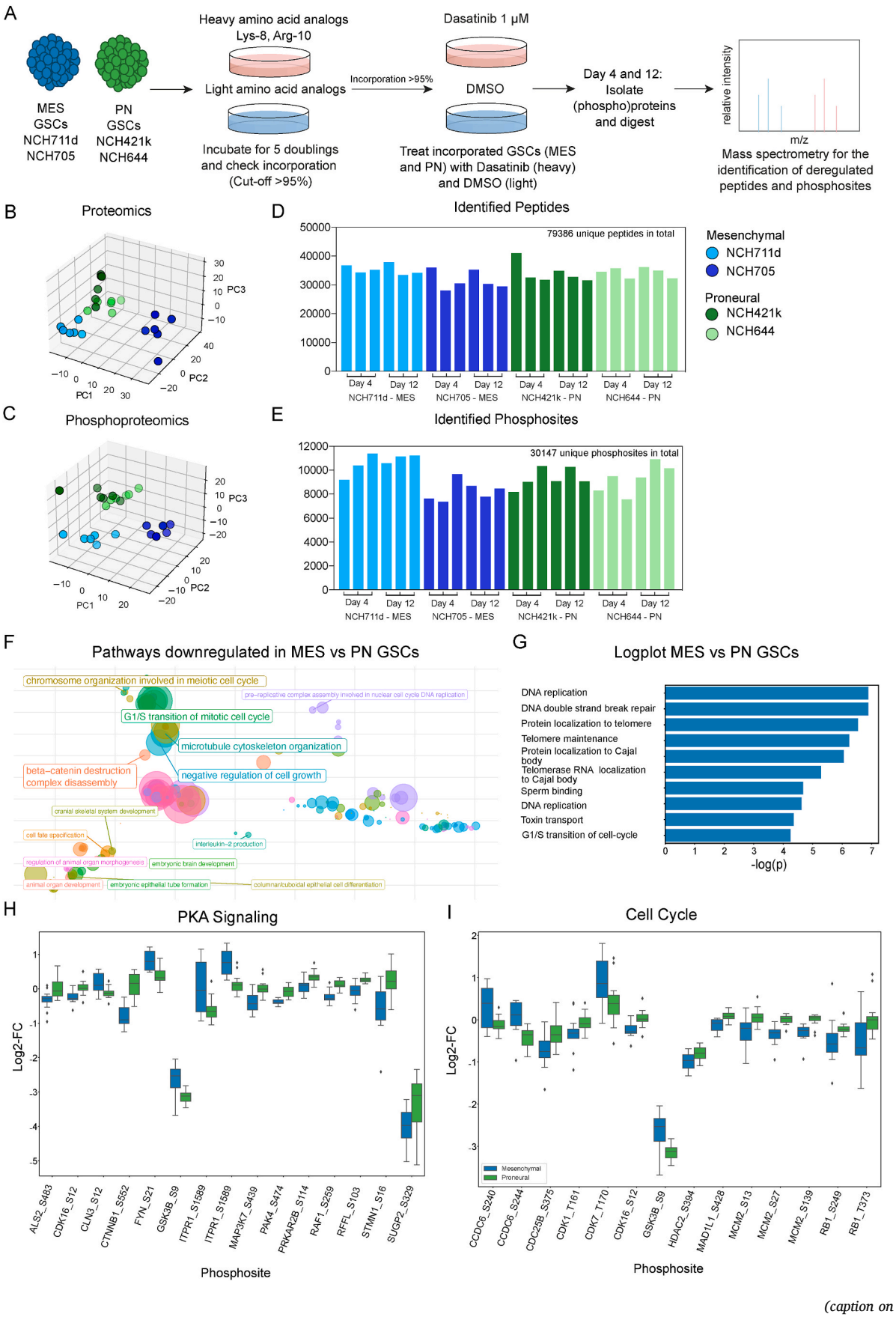


*(caption on next page)*

**Fig. 2.** Phosphoproteomics reveal reduced PKA and cell-cycle signaling after dasatinib inhibition in MES GSCs. (A) Scheme of the (phospho)proteomic screen. Initial analysis of 'heavy' samples revealed an incorporation rate of heavy proteins of over 95 % of total captured proteins. (B) 3D Principal Component Analysis (PCA) of GSCs after dasatinib inhibition. Included are replicates of (n = 3) day-4 and (n = 3) day-12 time point samples. PC = Principal Component. PCA for proteomics data. (C) Identified peptides for each sample (GSC and time point). (D) PCA for phosphoproteomics data. (E) Identified phosphosites for each sample (GSC and time point). (F) Simplot showing pathways significantly downregulated in MES (NCH711d and NCH705) but not PN (NCH421k and NCH644) GSCs upon 1 μM dasatinib inhibition. (G) p-values of the top 10 significantly downregulated pathways in MES and not PN GSCs. (H) Boxplot of Protein Kinase A (PKA) targets. Blue = MES, green = PN. Included are 15 phosphosites considered to be PKA targets by PhosphositePlus or Scansite that showed significant (adj-p <0.05) deregulation in PN compared to MES GSCs upon dasatinib inhibition (two-sided *t*-test). (I) Boxplot of cell cycle proteins. Blue = MES, green = PN. Significantly differential phosphosites related to cell cycle pathways are shown on the x-axis. MES = mesenchymal, PN = proneural, GSC = GB stem-like cell. PC = principal component. DMSO = Dimethuylsulfoxide.

### 3.2. Phosphoproteomics reveal PKA and CDK1 target proteins as possible mediators of dasatinib resistance in PN GB

After SILAC and subsequent inhibition with dasatinib, PN and MES GSCs underwent phosphoproteomic analysis using mass spectrometry. To that end, PN and MES GSCs marked with 'heavy' and 'light' amino acids were cultured with dasatinib and DMSO over a total period of 12 days (as a long-term endpoint - Fig. 2A, also see Supplementary Fig. 1A for heavy amino acid incorporation rates). An additional 4-day time point was used to elucidate the 'short-term' inhibition response. Separation between MES and PN samples was more pronounced in a principal component analysis (PCA) using phosphoproteomics compared to proteomics data. This is supported by our previous data that showed subtype-specific responses to dasatinib in GB [11]. Furthermore, samples on day 4 did not substantially vary from samples on day 12 after inhibition, neither on a proteomic, nor on a phosphoproteomic level (Fig. 2B and C). The processed output dataset included the relative quantification values of 1650 proteins and 1158 phosphoproteins from 24 samples (Fig. 2D and E, Supplementary Figs. 1B and 1C, Supplementary Table 1). We then compared the proteomic response to dasatinib between the MES and PN GSCs by analyzing the 1617 features that were detected in all samples and that map uniquely to a single protein. Using *TopGO*, we found that the 245 proteins down-regulated in MES but not PN GB are enriched in many gene sets related to translation (e. g. translational initiation, p = 6.7E-3) and the cell cycle (e. g. G1/S transition of mitotic cell cycle, p = 6.9E-5, Fig. 2F). When directly comparing MES and PN subtypes, we identified 197 proteins with a significantly different response to dasatinib (adj-p<0.01). Of these, 117 proteins showed a lower mean response in MES GSCs enriched for gene sets related to DNA replication initiation (p = 2.5E-5) and complex assembly involved with cell cycle DNA replication (p = 1.3E-7) (Fig. 2G, see Supplementary Fig. 2A and B for deregulations in MES GSCs, Supplementary Figs. 2C–F for deregulations in PN). On a phosphoproteomic level, hypergeometric tests using the PhosphositePlus database [24] were performed to determine whether the differentially deregulated phosphosites among the 1153 unique phosphopeptides identified in PN and MES GB are enriched for targets of particular kinases. Protein Kinase A (PKA) targets (adj-p = 0.039) and Protein Kinase C (PKC) targets (adj-p = 0.039) were both significantly overrepresented in the differential phosphosites, suggesting these kinases may have subtype-specific responses to dasatinib. Fig. 2H highlights the differential phosphosites that are targets of PKA based on the databases PhosphositePlus or Scansite [25]. We further investigated the phosphosites on genes related to the cell cycle (Fig. 2I). CDK1-T161, the activating phosphosite on CDK1 [26], and RB1-T373, the site on RB1 whose phosphorylation releases E2F and promotes the cell cycle [27], are both significantly downregulated by dasatinib in MES but not PN GSCs. Although these data suggest downregulation of the cell cycle in MES GSCs, we also observe significant upregulation of the activating phosphosite (T170) on key cell cycle protein CDK7 in mesenchymal cells [28]. Overall, these data indicate that key cell cycle phosphosites are affected substantially more in the dasatinib-sensitive MES than the dasatinib-resistant PN GSCs.

### 3.3. Pooled shRNA drop-out viability screen identifies WEE1 to sensitize PN GB to dasatinib inhibition

We used the Cellecta® shRNA DECIPHER® library to identify specific genes that affect dasatinib response in MES and PN GSCs. After shRNA lentiviral transduction, GSCs were randomized to dasatinib (or DMSO) treatment using their respective $IC_{20}$ concentration (Fig. 3A, Supplementary Table 3). Cell number and TagRFP-positivity in the GSCs were monitored to ensure a representation of the library, Supplementary Fig. 3A). Baseline samples (harvested at 18 h after transduction) and the dasatinib and DMSO endpoint samples of all screens were isolated, sequenced and deconvoluted to a read count of the corresponding shRNA. Internal controls revealed a low standard deviation for the range of reads in a given shRNA, indicating a good technical quality (Supplementary Fig. 3B). A separation between baseline, PN and MES GSCs was noted upon PCA analysis, supporting a subtype-dependent response to knockdowns via the DECIPHER® shRNA library. Another component of this separation was driven by dasatinib (Fig. 3B, Supplementary Figs. 4A and 4B). Analysis of fold changes within a given subtype revealed depletion of several genes in PN GCSs but not MES GCSs under dasatinib (Supplementary Table 3, Supplementary Fig. 4C), with significant top hits ranked according to their p-values (Fig. 3C, Supplementary Fig. 5). The top hit showing the lowest p-value (<0.0001) was the Wee1-like protein kinase (WEE1), a cell-cycle protein that acts as a negative regulator for entry into mitosis [29] and that has been shown to be pivotal to the survival of GSCs [30] (Fig. 3D).

### 3.4. Integration of proteomics and shRNA drop-out screen confirms WEE1 perturbation to sensitize PN GCSs to dasatinib

We used the computational SamNet 2.0 method to combine proteomics and shRNA screen data and hence prioritize top hits in resistant PN GCSs. SamNet 2.0 builds on ResponseNet [15] and SamNet [16] (Supplementary Fig. 6A) and provides two specific advantages compared to these earlier methods. First, high-degree hub nodes are penalized so that highly-connected proteins, like ubiquitin, do not dominate the network solution. Second, SamNet 2.0 allows for the incorporation of baseline expression data to produce more realistic optimal networks. To identify subtype-specific pathways, we treated MES and PN as separate commodities. We set up the directed graph (Fig. 4A) by connecting the source node (*S*) to 145 proteins significantly affected by dasatinib (adj-p<0.01 and abs($\log_2$FC) > 1) in each subtype separately (31 MES-specific proteins, 23 PN-specific proteins and 91 proteins represented in both subtypes). We connected the terminal sink node (*T*) to the 44 shRNA hits (16 MES-specific, 28 PN-specific) that cause a significantly different effect on depletion in the presence of dasatinib compared to DMSO (p < 0.05, and abs($\log_2$FC) > 1 compared to baseline). The proteomics and shRNA hits were then connected to identify an optimal protein-protein interaction network containing a small subset of proteins and *TopGO* was subsequently used to identify pathways enriched in this network. Many significantly enriched ontologies were related to the cell cycle, such as "G1/S transition of mitotic cell cycle" (p = 0.003) and "regulation of cell cycle" (p = 0.02, Supplementary Table 4). We assessed all 29 high quality networks and observed consistent enrichment for cell cycle related pathways in PN

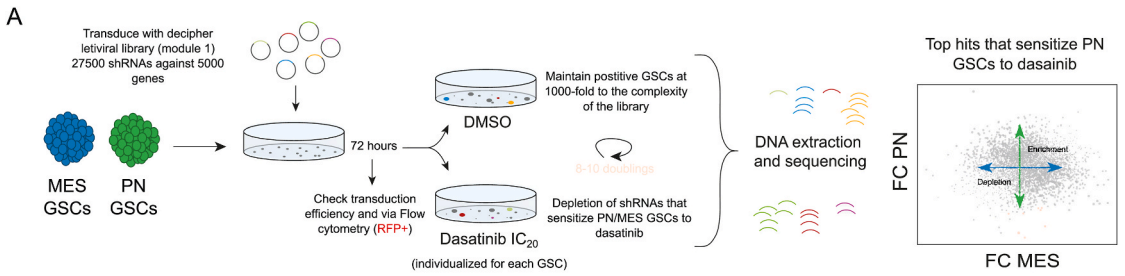


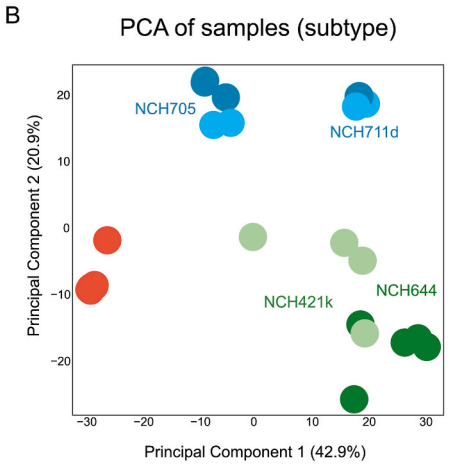


C

shRNA screen top 10 hits

| Gene | p-Value | MES logCPM foldchange | | | PN logCPM foldchange | | | MES vs PN |
|---|---|---|---|---|---|---|---|---|
| | | Dasatinib to Baseline | DMSO to Baseline | Dasatinib to DMSO | Dasatinib to Baseline | DMSO to Baseline | Dasatinib to DMSO | |
| WEE1 | 5.9E-05 | -0.707 | -0.617 | -0.09 | -1.595 | -0.367 | -1.228 | -1.138 |
| CREM | 0.00256 | -0.774 | -0.94 | 0.166 | -1.744 | -0.634 | -1.11 | -1.276 |
| RHOA | 0.00455 | -0.484 | -0.439 | -0.045 | -1.961 | -1.08 | -0.881 | -0.836 |
| ITGA3 | 0.00627 | -0.166 | 0.022 | -0.188 | -1.357 | -0.471 | -0.885 | -0.697 |
| MBD1 | 0.0066 | 0.065 | -0.069 | 0.133 | -0.913 | -0.13 | -0.783 | -0.916 |
| WNT8A | 0.00678 | -1.26 | -1.229 | -0.031 | -2.714 | -1.404 | -1.31 | -1.279 |
| SNCB | 0.008 | -0.417 | -0.54 | 0.123 | -1.999 | -1.178 | -0.821 | -0.944 |
| BPNT1 | 0.00879 | -0.398 | -0.498 | 0.1 | -1.148 | -0.36 | -0.789 | -0.889 |

Baseline | Dasatinib - MES | Dasatinib - PN | DMSO - MES | DMSO -PN

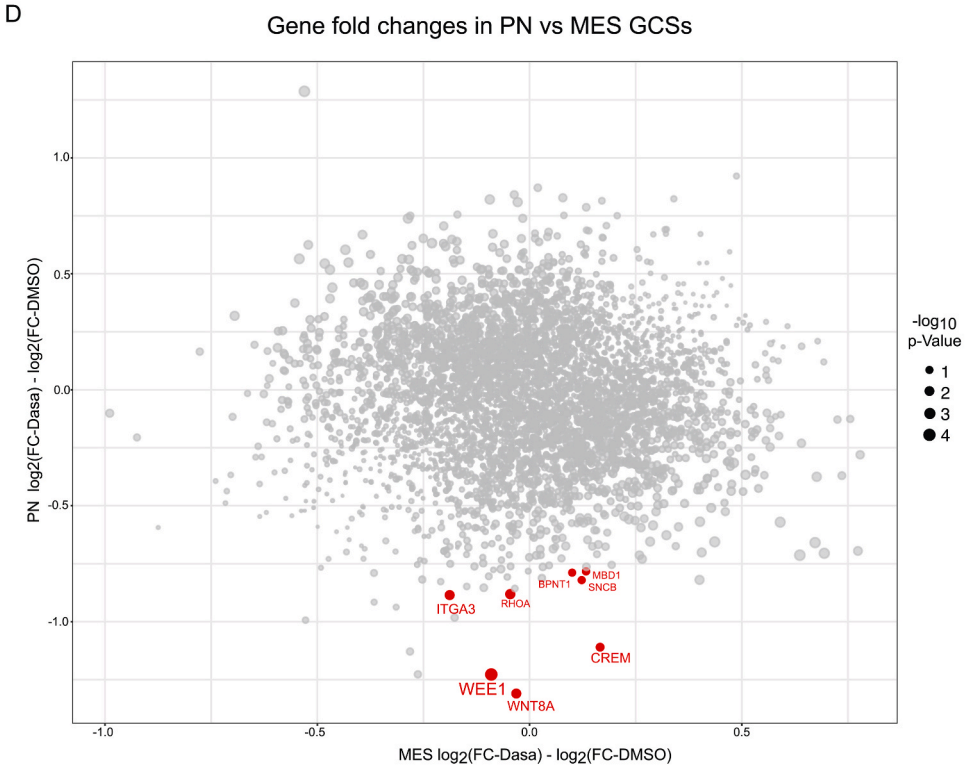


**Fig. 3.** Pooled shRNA drop-out viability screen reveals WEE1 to sensitize PN GB to dasatinib inhibition. (A) shRNA screen workflow. (B) Principal Component Analysis (PCA) of GSCs in pooled shRNA screen. MES = shades of blue, PN = shades of green. A general overview of the different GSC subtypes and screening conditions is provided, with islands of different GSC subtypes labelled. (C) Top hits of pooled barcoded shRNA screen. Shown are the p-values and logCPM read values for each condition (CPM = counts per million). Genes are ranked according to the p-value (dark green: lowest; white: highest). Negative foldchanges are represented by red bars, positive foldchanges by blue bars. (D) Dot plot of foldchanges of all genes targeted by the DECIPHER® screen. Shown is the difference in foldchange between the dasatinib and the DMSO screen in PN (y-axis) and MES (x-axis) GSCs. A PN hit is as close to 0 on the x-axis as possible and as negative on the y-axis as possible, provided it reaches significance (bigger dot sizes correspond to the lower p-values). Top hits from (C) are shown in red. FC = foldchange, Dasa = dasatinib. DMSO = Dimethyl sulfoxide.

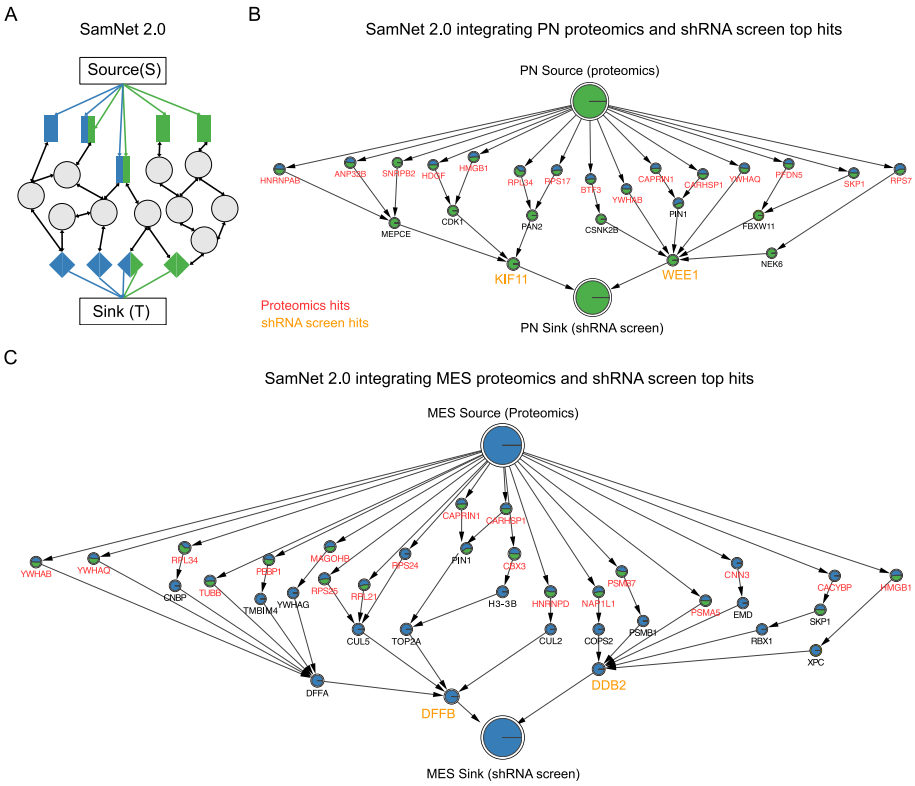


**Fig. 4.** Integration of phosphoproteomic data and DECIPHER® drop-out viability screen shows WEE1 as a target for synergistic combinational therapy in PN GSCs. (A) SamNet 2.0 directed graph. The graph begins with a source node (S) that has outgoing subtype-specific edges into nodes that represent proteins deregulated in response to dasatinib. These proteins are represented by rectangles (blue = MES-hit, green PN-hit, blue and green = deregulated in both. The gray nodes represent proteins not included in either screen, where each edge indicates a physical interaction between proteins. Since the interactions are bidirectional, the flow in the network can go either way. Diamonds at the end of the flow depict hits of the shRNA screen, with outgoing edges into the terminal sink node (T). (B) Cell cycle proteins connect vulnerabilities upon PN GSC dasatinib inhibition. Each node is divided into blue and green, depending on the PN (green) vs MES (blue) flow, with the size proportional to the node's share in total flow. Label colors represent the type of node: red is a proteomic hit, yellow/orange is an shRNA hit, and black is a non-hit protein from the PPI. (C) Optimal network yields DNA Damage Proteins in MES GSCs. Each node is divided into blue and green, depending on the PN (green) vs MES (blue) flow, with the size proportional to the node's share in total flow. Label colors represent the type of node as in B).

networks, such as the aforementioned "regulation of cell cycle" in 27/29 networks ($p < 0.05$). In the optimal network, many of nodes connect the differential proteins to the shRNA hits of WEE1 and KIF11 (Kinesin Family Member 11), which both play key roles in the cell cycle [31,32] (Fig. 4B). We also observed many interactions related to cell cycle regulation, such as 14-3-3 proteins (for example YWHAB - Tyrosine 3-Monooxygenase/Tryptophan 5-Monooxygenase) promoting WEE1 stability [33] and PIN1 (Peptidylprolyl Cis/Trans Isomerase, NIMA-Interacting 1) inactivating WEE1 [34,35] (Supplementary Table 4). MES-specific proteins enriched for pathways related to DNA damage, such as "nucleotide excision repair, DNA Damage Recognition" ($p = 3.0E-6$) and "apoptotic DNA fragmentation" ($p = 1.0E-4$, Fig. 4C–Supplementary Table 5).

### 3.5. *WEE1 inhibitor MK-1775 shows synergistic effects in combination with dasatinib in PN GSCs*

We performed inhibition experiments on PN and MES GSCs using dasatinib combined with MK-1775, a small molecular inhibitor of WEE1, to confirm the output of the integration dataset. Data analysis via SynergyFinder showed higher synergistic effects in PN GSCs with reduced cell viability 48 h after combination treatment (model-score $\delta = 23.05$ for NCH644, (Fig. 5A–B), and $\delta = 17.81$ for NCH421k, Supplementary Fig. 6B) compared to MES GSCs ($\delta = 4.97$ for NCH705, Fig. 5D–E, $\delta = 4.66$ for NCH711d, Supplementary Fig. 6C). Under the most synergistic concentrations, cell death was significantly higher in PN than MES GSCs at 48 and 96 h (Fig. 5F). Optimal combinatory doses of dasatinib and MK-1775 were similar when calculated using two different synergy models (zero interaction model and bliss independent model, Fig. 5G). Cerebral spheroids were utilized to further validate the robustness of this effect in a more complex tissue setting. The treatment of tumor-bearing (concomitantly luciferase- and GFP-expressing NCH644) cerebral spheroid co-culture was performed in two separate experiments (4-day and 8-day inhibition), including four conditions: Vehicle control, single dasatinib and MK-1775 treatments and a dasatinib and MK-1775 combination therapy (Fig. 5H). A significant reduction of tumor growth in the combination treatment group compared to single treatment and vehicle was observed over time (Fig. 5I and Supplementary Fig. 6D). Strikingly, while tumor growth under MK-1775 was only marginally different to the combination therapy 4 days post-treatment, further observation at day 8 and 12 showed a divergence in tumor size between the combination and single MK-1775 therapy, with the former showing complete eradication of tumor cells at day 12 post-treatment. In line with the bioluminescence measurements, GFP and Nestin quantified via Immunofluorescence (IF) at day 4 post-treatment showed a significant reduction in signal under combination therapy compared to the other groups, indicative of depletion of NCH644 GCSs within the co-culture (Fig. 5J–L). Ki67 expression showed a similar effect, indicating reduced proliferation under combination therapy (Supplementary Fig. 6E).

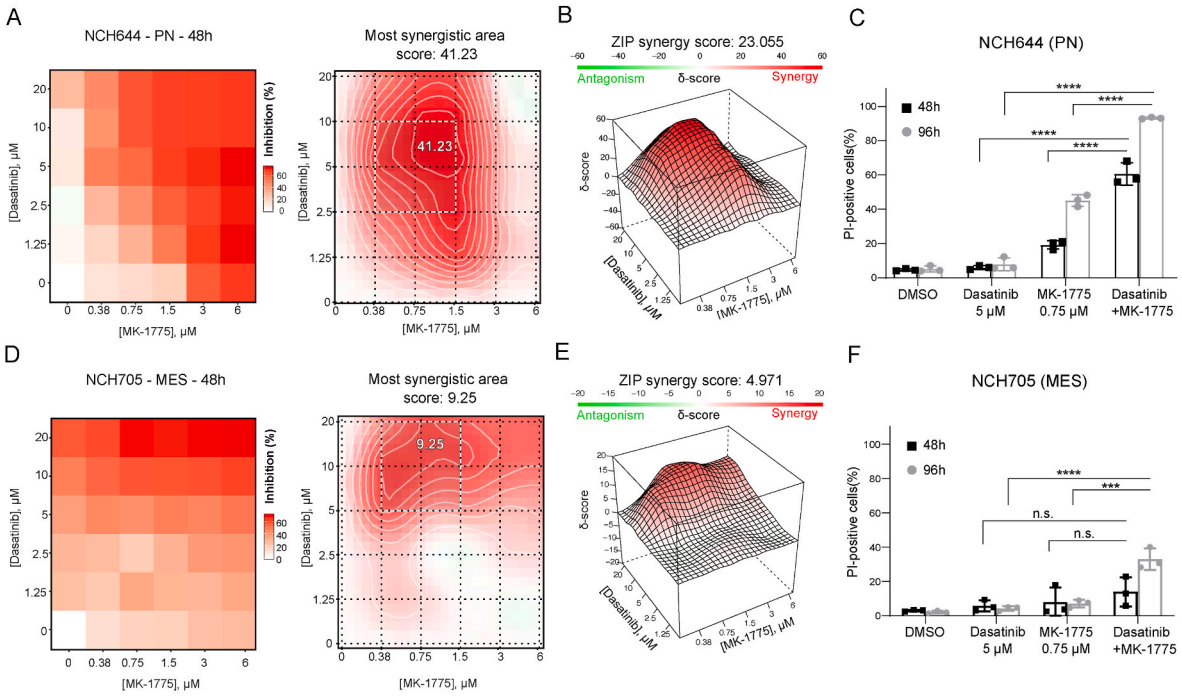


G

| Synergy scores in GCSs | | Zero interaction model | | | | Bliss independence model | | | |
|---|---|---|---|---|---|---|---|---|---|
| | | Most synergistic area score | Dasatinib [μM] | MK-1775 [μM] | Synergy score | Most synergistic area score | Dasatinib [μM] | MK-1775 [μM] | Synergy score |
| PN | NCH644 | 41.23 | 5 | 0.75 | 23.05 | 40.97 | 5 | 0.75 | 23.03 |
| | NCH421k | 27.91 | 2.5 | 1.5 | 17.81 | 28.04 | 5 | 1.5 | 17.66 |
| MES | NCH705 | 9.25 | 10 | 0.75 | 4.97 | 9.32 | 10 | 0.75 | 4.66 |
| | NCH711d | 12.41 | 2.5 | 0.75 | 4.66 | 11.64 | 2.5 | 0.75 | 4.68 |

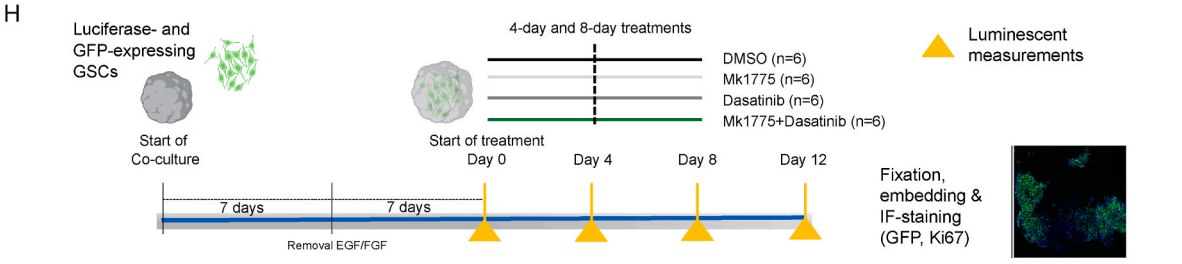


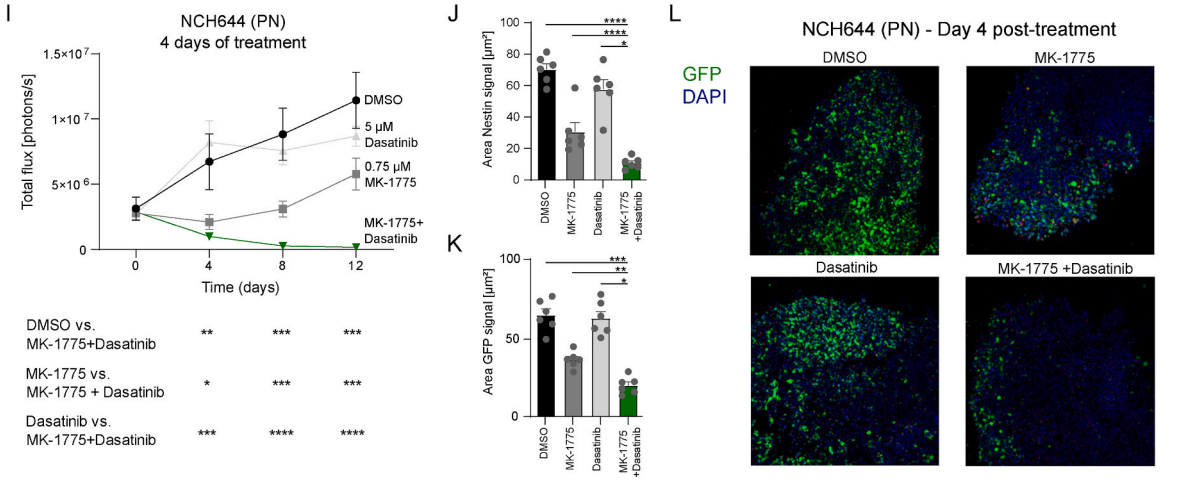


*(caption on next page)*

**Fig. 5.** Synergistic dasatinib and WEE1 inhibition in PN GCSs. (A) Dose-response viability plot with matrix plot showing concentrations with the most synergistic area and (B) Synergy score (δ) based on the ZIP (zero interaction potency) model after dasatinib and MK-1775 treatment depicting synergistic effects of dasatinib and MK-1775 in PN NCH644. GSCs were treated with different concentrations of dasatinib (1.25–20 μM) and MK-1775 (0.375–6 μM) for 48 h. Cell viability was determined via CellTiter-Glo® assay (n = 3). Red denotes synergism, green denotes antagonism (n = 3). (C) Propidium-iodide (PI) staining 48h (black) and 96h (gray) after treatment of PN NCH644 GSCs with the combination dose showing the highest synergistic score (5 μM dasatinib, 0.75 μM MK-1775), with controls using vehicle (DMSO: Dimethylsulfoxide) and single treatments of dasatinib and the WEE1 inhibitor MK-1775 (n = 3). (D) Dose-response viability plot with matrix plot and E) Synergy score (δ) based on the ZIP model MES NCH705. (F) PI staining 48h (black) and 96h (gray) after treatment of PN NCH644 GSCs with the combination dose showing the highest synergistic score with different controls (n = 3). (G) Depiction of the most optimal combination concentrations with calculated synergy scores as determined by the ZIP and BLISS independence model in all GSCs. (H) Experimental set-up and treatment intervals of the NCH644 cerebral spheroid co-culture experiment with 5 μM dasatinib, 0.75 μM MK-1775 and a combination. (I) Luminescence intensity of photons emitted from each spheroid as a surrogate measure for response to 96h treatment in four groups, measured at treatment start (day 0) followed by measurements every 96h for a total of 12 days. Six spheroids were used per condition, p-values for different time points are indicated under the graph, two-way ANOVA corrected with Tukey's test for multiple comparisons was used. (J) Quantification of anti-GFP and (K) Anti-nestin staining signals upon different treatment modalities as indicated at day 4 after treatment. Signal was normalized to number of cells (based on DAPI). Error bars depict standard error of the mean (SEM), *p < 0.05, **p < 0.01, ***p < 0.001, ****p < 0.0001, n.s.: not significant, one-way ANOVA corrected with Tukey's test for multiple comparisons. (L) Representative images after day 4 of treatment showing GFP and DAPI signals in co-culture spheroids under different treatment conditions. Co-culture spheroids were stained with anti-GFP marking tumor cells (green) and DAPI was used as a DNA marker (blue) to correct for different co-culture spheroid sizes. 6 spheroids were used per condition and 2-3 slices per spheroid.

### *3.6. Cell cycle regulation could explain differences in WEE1 inhibition efficacy in PN and MES GSCs*

Given the relevance of WEE1 and cell cycle proteins for subtype-specific dasatinib response, we characterized the nature of WEE1 expression across GSC subtypes and normal brain. On a protein level, WEE1 showed significantly higher expression in PN GCSs compared to MES GCSs and astrocytes (Fig. 6A). When examining The Cancer Genome Atlas (TCGA) dataset, GB patient tumors showed a higher RNA expression of *WEE1* RNA to normal brain tissue (Fig. 6B). However, RNA-Seq data of GB patients showed *WEE1* expression to be the lowest in the PN subtype compared to other subtypes (Fig. 6C) and in our GSC model, no differences were noted in the mRNA levels of *WEE1* between MES and PN GSCs (Fig. 6D, measured by gene expression profiling [GEO accession: GSE159609] see Supplementary Fig. 7A for MES- and PN-specific *OLIG2* and *CD44* expression) This discrepancy between WEE1 protein and mRNA levels highlights the importance of proteomics in the context of this study. To provide a mechanistic explanation for the differences observed between PN and MES GSCs, we examined the extent of the activating WEE1-mediated CDK1 phosphorylation in both subtypes, and the effects of dasatinib or MK-1775 on this phosphosite (Y15). Notably, both total and phosphorylated CDK1 levels were higher in PN GSCs, confirming the observations from the phosphoproteomic data. As expected, given that CDK1 is the direct substrate of WEE1, MK-1775 dramatically reduced CDK1 phosphorylation in both subtypes, whereas dasatinib appeared to reduce CDK1 phosphorylation in MES but not PN GCSs (Fig. 6E). This potentially explains the resistance of PN GSCs to dasatinib treatment that could be attributable to differences in cell-cycle regulation between the PN and MES subtypes. By applying a GOBP (Gene Ontology Biological Process) cell-cycle signature on TCGA GB patient RNA-Seq data from tumor samples of different subtypes (CL, PN and MES), we noticed a subtype-based clustering pattern, with a statistically significant MES-dominated cluster (p-value = 6.266e-09, Fisher's exact test, Fig. 6F). This was also apparent through different patterns of alignment on Uniform Manifold Approximation and Projection (UMAP) plots (Fig. 6G, UMAP1 + UMAP2 embedding values of MES tumors were significantly different from other subtypes, Mann-Whitney *U* test, Supplementary Fig. 7B). Furthermore, the combination of dasatinib and MK-1775 for 48 h leads to an accumulation of cells in both the G2/M and the S-phases of the cell cycle with an accompanying drop in cells in the G1 phase in PN GSCs but not MES GSCs (Fig. 6H and Supplementary Fig. 7 C-F). This could indicate that while some cells are being forced to progress through the cycle, others are stalling in S-phase due to the combined stress from DNA damage and the effects of the inhibitors. This dual action could lead to a paradoxical accumulation of cells in S-phase, as the cells are unable to effectively complete DNA replication or repair damage. Taken together, these data highlight the implication of the differential cell cycle regulation in PN and MES GCSs in manifesting the selectively damaging effects of combined WEE1 and dasatinib inhibition in PN GCSs. As WEE1 usually serves to shield cells from mitotic catastrophe by preventing G2/M transition of cells harboring fulminant DNA damage [36], we tested the hypothesis as to whether this could explain the sensitivity observed in PN GCSs. Indeed, treatment with combination of dasatinib and MK-1775 induces higher levels of γH2Ax in PN than MES GSCs, suggesting higher levels of DNA damage in PN GCSs through the combination (Fig. 6I).

## 4. Discussion

Combination therapies can provide a promising option for tumor eradication, especially in the case of GB, where tumor heterogeneity and swiftly emerging resistance to treatment underscore the importance of addressing multiple facets of tumor biology to consolidate longer responses to therapy. We previously observed that MES GSCs were sensitive and PN GSCs particularly resistant to dasatinib *in vitro*. This is why identifying potential combination therapy targets to improve the efficacy in PN GSCs and in doing this, unravelling possible subtype-specific response, is of paramount importance. To accomplish this, we collected phospho(proteomic) data to characterize response to dasatinib in PN and MES GSCs and performed a loss-of-function shRNA screen to identify potential targets for therapy. We then developed a novel computational approach to integrate different data inputs and help prioritize shRNA screen hits for functional validation.

Network analyses have been previously used to determine pathway vulnerabilities in oncological diseases [15,37]. The method implemented in this work (SamNet 2.0) significantly improves the existing network flow ResponseNet and SamNet flow algorithms. Specifically, it prevents highly-connected proteins from dominating the flow pattern and curates gene expression data to yield more realistic 'solutions'. This approach particularly fits the datasets at hand since not all human genes are captured by proteomics or targeted by shRNA data. By 'filling the gaps', this network integration approach allowed for connecting the strongest hits from these two assays through additional potentially relevant genes. SamNet 2.0 revealed significant flow through cell cycle genes and into the WEE1 node for the PN subtype, highlighting this as a priority for validation experiments.

On a molecular level, WEE1 phosphorylates and thereby inhibits CDK1 [38], thus inducing a G2-M cell-cycle checkpoint arrest. This is particularly relevant for cancer cells as they tend to have deficiencies in the G1-S checkpoint and depend on a functional G2-M checkpoint for DNA repair before mitotic entry [29]. WEE1 has indeed been implicated in the growth and progression of breast cancer, leukemia, and glioblastoma [39].

In addition to the computational integration of proteomics and the shRNA loss-of-function screen, this study was further complemented by phosphoproteomic data. Phosphoproteomic profiling is indeed useful in

characterizing the cell kinome in the context of inhibition by targeted therapy with kinase inhibitors like dasatinib. In this study, comparing PN (resistant) to MES (sensitive) GSCs showed a reduction of CDK1 target phosphorylations and in turn cell cycle-related pathways in MES and not PN GSCs. Indeed, CDK1 target phosphorylations, particularly those associated with cell cycle signaling, are not suppressed under

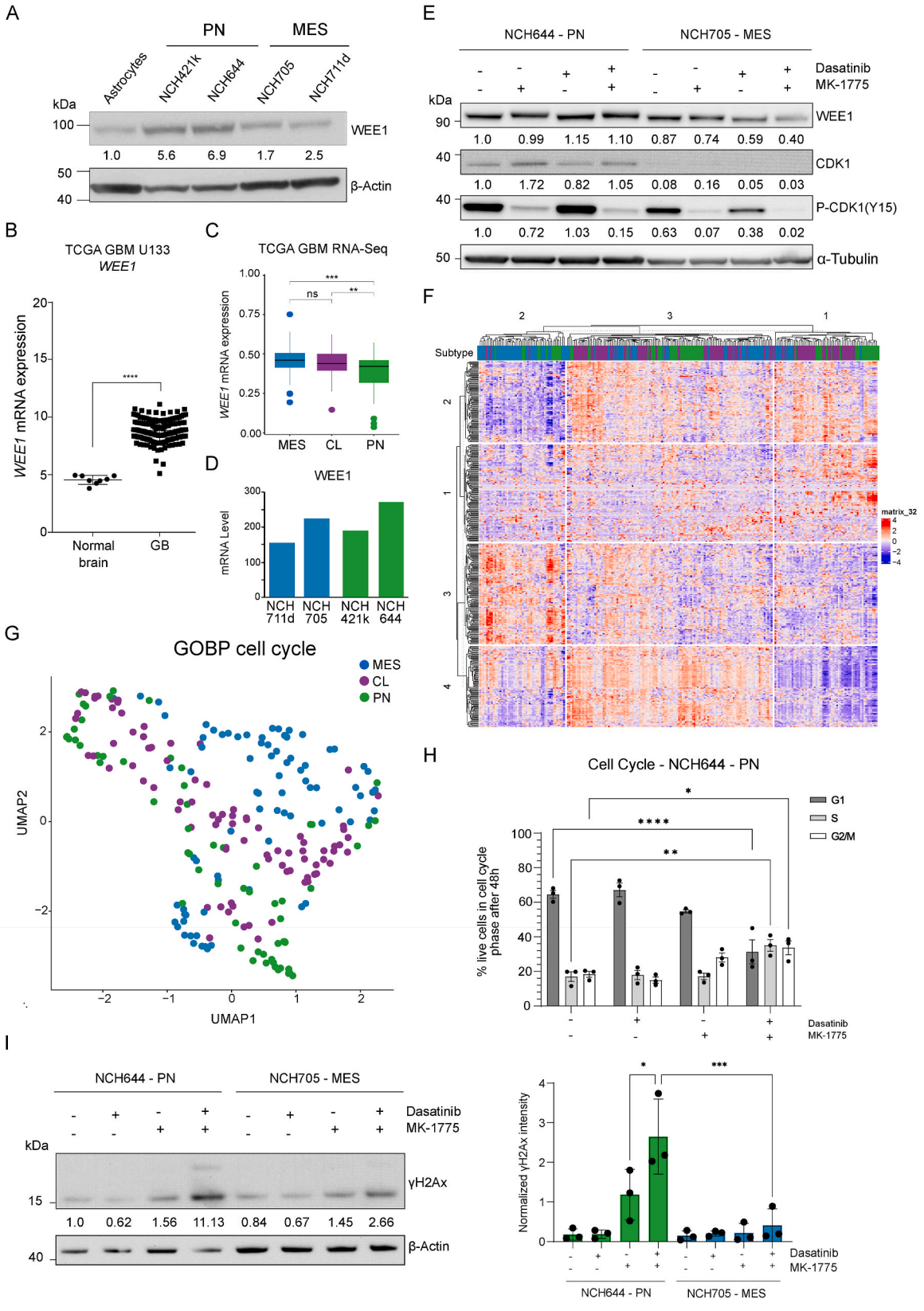


*(caption on next page)*

**Fig. 6.** PN GCSs show a different WEE-1 mediated cell-cycle regulation pattern. (A) Western blot showing WEE1 protein levels in astrocytes and PN (NCH421k, NCH644) and MES (NCH705, NCH711d) GSC subtypes. β-Actin served as a loading control. Band intensities are shown, normalized to β-Actin and then to astrocytes (B) *WEE1* mRNA expression in GB compared to normal brain tissue (data from Ref. [50], unpaired student's t-test, ****$p < 0.0001$). (C) Boxplots showing TCGA GB RNA-Seq *WEE1* expression in MES, CL and PN GB patient samples ***$p < 0.001$, **$p < 0.01$. (D) mRNA levels of *WEE1* in the MES and PN GSC subtypes from gene expression profiling data (GEO accession: GSE159609). E) Western blot showing protein levels of WEE1, CDK1, and P-CDK in DMSO (−/−), dasatinib (5 μM) and MK-1775 (0.75 μM) single or in combination treated PN NCH644 and MES NCH705 cells (48 h), α-tubulin served as a loading control. Band intensities are shown, normalized to α-tubulin and then to the PN DMSO samples. (F) Heatmap with unsupervised clustering analysis of the TCGA GB RNA-Seq data patient cohort reclassified according to the signatures (n = 265), showing 3 clustering groups with patterns of subtype-dependent clustering upon calling genes of GOBP Cell Cycle signature. Patient samples are distributed horizontally, with colors denoting GB subtype, genes from the gene set are listed vertically. (G) Uniform Manifold Approximation and Projection (UMAP) plot showing TCGA GB RNA-Seq patient sample distribution of different subtypes (MES, CL, PN) upon calling genes of the GOBP Cell Cycle signature. (H) Assessment of cell cycle phases by using PI-staining as measured by FACS in PN (NCH644) after treatment with DMSO (−/−), 5 μM dasatinib, 0.75 μM MK-1775 or the combination for 48 h, data shown after excluding live cells (subG1 phase was removed). Significances are displayed for DMSO treatment comparisons (mean ± SEM, p-values are indicated in the graph, two-way ANOVA corrected with Tukey's test for multiple comparisons, *<0.05, **<0.01*** < 0.001, **** <0.0001, NCH644 n = 3. (I) (Left) Representative Western blot showing protein levels of γH2Ax in PN NCH644 and MES NCH705 GCSs 48h after dasatinib (5 μM) and MK-1775 (0.75 μM) combination or single-treatments or with DMSO (−/−), β-Actin served as a loading control. MES = mesenchymal, PN = proneural, CL = classical. (Right) Quantification of band intensities from three independent experiments, mean ± SD, one-way ANOVA corrected with Tukey's test for multiple comparisons, *<0.05, ***<0.001.

dasatinib in PN GCSs. Since CDK1 is also a well-known regulator of the cell cycle at its G2/M phase transition [40] and is regulated by WEE1, this further strengthened the hypothesis that WEE1 activity could explain the persistence of PN GSCs under dasatinib. CDK1 has been previously studied for inhibition in cancer [41] and implicated in shorter survival in GB [42]. A further important observation of the phosphoproteomic profiling was revealed through the global comparison of 4-day vs 12-day samples after dasatinib inhibition, showing no substantial differences between time points and suggesting that resistance mechanisms manifest at a relatively early timepoint of inhibition, which is in line with what has been previously reported in GB [43].

A previous phosphoproteomic screen has shown that WEE1 inhibition exposes a vulnerability in PN GB cell lines when compared to normal brain (no other subtypes were included in the study) [44]. In our work we have shown through *in vitro* and tumor-bearing cerebral spheroid experiments why combination with dasatinib is more effective. Firstly, this effect was shown to be specific to PN GSCs when compared to the MES subtype. Secondly, the synergistic value of applying dasatinib and MK-1775 compared to monotherapy was shown, and thirdly, as shown in tumor-bearing spheroid experiments for the same treatment interval, tumor growth was thwarted in combination therapy (up to day 12) compared to monotherapy with the WEE1 inhibitor MK-1775, where tumor growth resumed after the end of exposure.

Regarding the observed synergy, WEE1 has been implicated to be part of a wider resistance adaptation after PI3K inhibition, a pathway that also interacts with the SRC pathway (inhibited by dasatinib), since both are involved in mediating signals of growth factor receptors [5,45]. However, a previous report of kinase gene expression analysis showed how the inhibition of WEE1 sensitizes GB to ionizing radiation and postulated that WEE1 could save cells from a 'mitotic catastrophe' [36]. This hypothesis was extended to the combination of WEE1 inhibitors and DNA-damaging agents in general [46]. Since dasatinib, along with kinase inhibition, has been shown to cause DNA damage in many tumor entities [47], it is reasonable to suggest that adding WEE1 inhibition to dasatinib could enhance its DNA-damaging effects, as previously demonstrated in Burkitt lymphoma [48]. Indeed, the combination of dasatinib and WEE1 inhibition, as applied in this study, has also been mechanistically linked to DNA damage potentiation in ovarian cancer [49].

Congruent to these observations, increased yH2Ax levels, indicative of DNA damage, and accumulation of cells in the G2/M and S-phase of the cell cycle, were noted after combination of dasatinib and the WEE1 inhibitor in PN compared to MES GSCs, hinting towards a higher level of DNA damage in the PN cells. Because RNA-Seq GB patient data analysis shows how PN and MES subtypes demonstrate divergent expression of cell cycle genes indicative of a different pattern of cell-cycle regulation, it could be conceivable that this differential and apparently WEE1-vulnerable PN GB cell cycle regulation could be exploited to propagate DNA damage through combination with the otherwise ineffective dasatinib, driving PN GCSs into mitotic catastrophe. In the real-world setting of a heterogeneous tumor, concomitant WEE1 inhibition and dasatinib treatment could therefore provide an effective combination to address both the dasatinib-sensitive MES and the combination-sensitive PN-subpopulations in a GB tumor.

## 5. Conclusion

This work highlights useful methods that are crucial for understanding cancer resistance, such as (phospho)proteomics and functional shRNA screens. Additionally, we show the utility of computational integration for prioritizing future validation experiments and reveal possible targets for synergistic therapy of dasatinib and targeting WEE1 in proneural Glioblastoma. With substantial heterogeneity in many tumor entities, our findings detail a useful approach that can be repurposed and modified in other studies to investigate subtype-specific drug effects in other cancer entities.

## Funding

O.T.A. was financed by a stipend of the Heinrich F.C. Behr Trust. This work was supported by the Deutsche Forschungsgemeinschaft (DFG, German Research Foundation) – Project-ID 404521405, SFB 1389 - UNITE Glioblastoma and NIH/NIH U01CA253547.

## Ethics approval

The relevant research proposals for work on the GSCs and the analyses of patients' samples included were approved by the Institutional Review Board at the Medical Faculty of Heidelberg.

## Availability of data and materials

Proteomics data are available under the Proteomics Identification database (PRIDE) via ProteomeXchange with identifier PXD039264. All data generated or analyzed during this study are included in this published article and its supplementary information files. Codes used for bioinformatics analyses are available upon reasonable request.

## CRediT authorship contribution statement

**Obada T. Alhalabi:** Writing – review & editing, Writing – original draft, Validation, Resources, Methodology, Investigation, Data curation, Conceptualization. **Mona Göttmann:** Writing – original draft, Validation, Investigation, Formal analysis, Data curation. **Maxwell P. Gold:** Writing – original draft, Visualization, Software, Resources, Formal analysis, Data curation, Conceptualization. **Silja Schlue:** Investigation,

Formal analysis. **Thomas Hielscher:** Software, Formal analysis. **Murat Iskar:** Visualization, Software, Project administration. **Tobias Kessler:** Supervision, Resources. **Ling Hai:** Visualization, Formal analysis. **Tolga Lokumcu:** Methodology. **Clara C. Cousins:** Visualization, Software, Formal analysis. **Christel Herold-Mende:** Resources. **Bernd Heßling:** Visualization, Validation, Methodology, Investigation. **Sandra Horschitz:** Validation. **Ammar Jabali:** Visualization, Validation. **Philipp Koch:** Supervision. **Ulrich Baumgartner:** Validation. **Bryan W. Day:** Resources, Formal analysis. **Wolfgang Wick:** Supervision. **Felix Sahm:** Supervision. **Sandro M. Krieg:** Supervision. **Ernest Fraenkel:** Supervision, Methodology. **Emma Phillips:** Writing – review & editing, Writing – original draft, Validation, Supervision, Funding acquisition, Data curation. **Violaine Goidts:** Writing – review & editing, Writing – original draft, Project administration, Funding acquisition, Formal analysis, Conceptualization.

## Declaration of competing interest

The authors declare that they have no known competing financial interests or personal relationships that could have appeared to influence the work reported in this paper.

## Acknowledgements

Thanks to Lea Hansen Palmus, Kathrin Schramm, David T. W. Jones, Sevin Turcan, Frederik Bethke, Laura Puccio and Gabriele Müller for assisting with experiments and expertise. The mass spectrometry protein analysis was carried out by the DKFZ Proteomics Core Facility (PCF – Dr. Dominic Helm).

## Appendix A. Supplementary data

Supplementary data to this article can be found online at https://doi.org/10.1016/j.canlet.2024.217265.

## References

[1] D.N. Louis, A. Perry, G. Reifenberger, A. von Deimling, D. Figarella-Branger, W. K. Cavenee, H. Ohgaki, O.D. Wiestler, P. Kleihues, D.W. Ellison, The 2016 world health organization classification of tumors of the central nervous system: a summary, Acta Neuropathol. 131 (2016) 803–820.

[2] M. Weller, M. van den Bent, M. Preusser, E. Le Rhun, J.C. Tonn, G. Minniti, M. Bendszus, C. Balana, O. Chinot, L. Dirven, P. French, M.E. Hegi, A.S. Jakola, M. Platten, P. Roth, R. Rudà, S. Short, M. Smits, M.J.B. Taphoorn, A. von Deimling, M. Westphal, R. Soffietti, G. Reifenberger, W. Wick, EANO guidelines on the diagnosis and treatment of diffuse gliomas of adulthood, Nat. Rev. Clin. Oncol. 18 (2021) 170–186.

[3] C.W. Brennan, R.G. Verhaak, A. McKenna, B. Campos, H. Noushmehr, S.R. Salama, S. Zheng, D. Chakravarty, J.Z. Sanborn, S.H. Berman, R. Beroukhim, B. Bernard, C. J. Wu, G. Genovese, I. Shmulevich, J. Barnholtz-Sloan, L. Zou, R. Vegesna, S. A. Shukla, G. Ciriello, W.K. Yung, W. Zhang, C. Sougnez, T. Mikkelsen, K. Aldape, D.D. Bigner, E.G. Van Meir, M. Prados, A. Sloan, K.L. Black, J. Eschbacher, G. Finocchiaro, W. Friedman, D.W. Andrews, A. Guha, M. Iacocca, B.P. O'Neill, G. Foltz, J. Myers, D.J. Weisenberger, R. Penny, R. Kucherlapati, C.M. Perou, D. N. Hayes, R. Gibbs, M. Marra, G.B. Mills, E. Lander, P. Spellman, R. Wilson, C. Sander, J. Weinstein, M. Meyerson, S. Gabriel, P.W. Laird, D. Haussler, G. Getz, L. Chin, The somatic genomic landscape of glioblastoma, Cell 155 (2013) 462–477.

[4] D. Sturm, H. Witt, V. Hovestadt, D.A. Khuong-Quang, D.T. Jones, C. Konermann, E. Pfaff, M. Tonjes, M. Sill, S. Bender, M. Kool, M. Zapatka, N. Becker, M. Zucknick, T. Hielscher, X.Y. Liu, A.M. Fontebasso, M. Ryzhova, S. Albrecht, K. Jacob, M. Wolter, M. Ebinger, M.U. Schuhmann, T. van Meter, M.C. Fruhwald, H. Hauch, A. Pekrun, B. Radlwimmer, T. Niehues, G. von Komorowski, M. Durken, A. E. Kulozik, J. Madden, A. Donson, N.K. Foreman, R. Drissi, M. Fouladi, W. Scheurlen, A. von Deimling, C. Monoranu, W. Roggendorf, C. Herold-Mende, A. Unterberg, C.M. Kramm, J. Felsberg, C. Hartmann, B. Wiestler, W. Wick, T. Milde, O. Witt, A.M. Lindroth, J. Schwartzentruber, D. Faury, A. Fleming, M. Zakrzewska, P.P. Liberski, K. Zakrzewski, P. Hauser, M. Garami, A. Klekner, L. Bognar, S. Morrissy, F. Cavalli, M.D. Taylor, P. van Sluis, J. Koster, R. Versteeg, R. Volckmann, T. Mikkelsen, K. Aldape, G. Reifenberger, V.P. Collins, J. Majewski, A. Korshunov, P. Lichter, C. Plass, N. Jabado, S.M. Pfister, Hotspot mutations in H3F3A and IDH1 define distinct epigenetic and biological subgroups of glioblastoma, Cancer Cell 22 (2012) 425–437.

[5] Q. Wang, B. Hu, X. Hu, H. Kim, M. Squatrito, L. Scarpace, A.C. deCarvalho, S. Lyu, P. Li, Y. Li, F. Barthel, H.J. Cho, Y.H. Lin, N. Satani, E. Martinez-Ledesma, S. Zheng, E. Chang, C.E. Gabriel Sauve, A. Olar, Z.D. Lan, G. Finocchiaro, J.J. Phillips, M. S. Berger, K.R. Gabrusiewicz, G. Wang, E. Eskilsson, J. Hu, T. Mikkelsen, R. A. DePinho, F. Muller, A.B. Heimberger, E.P. Sulman, D.H. Nam, R.G.W. Verhaak, Tumor evolution of glioma-intrinsic gene expression subtypes associates with immunological changes in the microenvironment, Cancer Cell 33 (2018) 152.

[6] C. Neftel, J. Laffy, M.G. Filbin, T. Hara, M.E. Shore, G.J. Rahme, A.R. Richman, D. Silverbush, M.L. Shaw, C.M. Hebert, J. Dewitt, S. Gritsch, E.M. Perez, L. N. Gonzalez Castro, X. Lan, N. Druck, C. Rodman, D. Dionne, A. Kaplan, M. S. Bertalan, J. Small, K. Pelton, S. Becker, D. Bonal, Q.D. Nguyen, R.L. Servis, J. M. Fung, R. Mylvaganam, L. Mayr, J. Gojo, C. Haberler, R. Geyeregger, T. Czech, I. Slavc, B.V. Nahed, W.T. Curry, B.S. Carter, H. Wakimoto, P.K. Brastianos, T. T. Batchelor, A. Stemmer-Rachamimov, M. Martinez-Lage, M.P. Frosch, I. Stamenkovic, N. Riggi, E. Rheinbay, M. Monje, O. Rozenblatt-Rosen, D.P. Cahill, A.P. Patel, T. Hunter, I.M. Verma, K.L. Ligon, D.N. Louis, A. Regev, B.E. Bernstein, I. Tirosh, M.L. Suvà, An integrative model of cellular states, plasticity, and genetics for glioblastoma, Cell 178 (2019) 835–849.e821.

[7] J. Klughammer, B. Kiesel, T. Roetzer, N. Fortelny, A. Nemc, K.H. Nenning, J. Furtner, N.C. Sheffield, P. Datlinger, N. Peter, M. Nowosielski, M. Augustin, M. Mischkulnig, T. Ströbel, D. Alpar, B. Ergüner, M. Senekowitsch, P. Moser, C. F. Freyschlag, J. Kerschbaumer, C. Thomé, A.E. Grams, G. Stockhammer, M. Kitzwoegerer, S. Oberndorfer, F. Marhold, S. Weis, J. Trenkler, J. Buchroithner, J. Pichler, J. Haybaeck, S. Krassnig, K. Mahdy Ali, G. von Campe, F. Payer, C. Sherif, J. Preiser, T. Hauser, P.A. Winkler, W. Kleindienst, F. Würtz, T. Brandner-Kokalj, M. Stultschnig, S. Schweiger, K. Dieckmann, M. Preusser, G. Langs, B. Baumann, E. Knosp, G. Widhalm, C. Marosi, J.A. Hainfellner, A. Woehrer, C. Bock, The DNA methylation landscape of glioblastoma disease progression shows extensive heterogeneity in time and space, Nat. Med. 24 (2018) 1611–1624.

[8] B. Campos, Z. Gal, A. Baader, T. Schneider, C. Sliwinski, K. Gassel, J. Bageritz, N. Grabe, A. von Deimling, P. Beckhove, C. Mogler, V. Goidts, A. Unterberg, V. Eckstein, C. Herold-Mende, Aberrant self-renewal and quiescence contribute to the aggressiveness of glioblastoma, J. Pathol. 234 (2014) 23–33.

[9] J. Chen, Y. Li, T.S. Yu, R.M. McKay, D.K. Burns, S.G. Kernie, L.F. Parada, A restricted cell population propagates glioblastoma growth after chemotherapy, Nature 488 (2012) 522–526.

[10] S. Bao, Q. Wu, R.E. McLendon, Y. Hao, Q. Shi, A.B. Hjelmeland, M.W. Dewhirst, D. D. Bigner, J.N. Rich, Glioma stem cells promote radioresistance by preferential activation of the DNA damage response, Nature 444 (2006) 756–760.

[11] O.T. Alhalabi, M.N.C. Fletcher, T. Hielscher, T. Kessler, T. Lokumcu, U. Baumgartner, E. Wittmann, S. Schlue, M. Göttmann, S. Rahman, L. Hai, L. Hansen-Palmus, L. Puccio, I. Nakano, C. Herold-Mende, B.W. Day, W. Wick, F. Sahm, E. Phillips, V. Goidts, A novel patient stratification strategy to enhance the therapeutic efficacy of dasatinib in glioblastoma, Neuro Oncol. (2021).

[12] J.S. Khorashad, A.M. Eiring, C.C. Mason, K.C. Gantz, A.D. Bowler, H.M. Redwine, F. Yu, I.L. Kraft, A.D. Pomicter, K.R. Reynolds, A.J. Iovino, M.S. Zabriskie, W. L. Heaton, S.K. Tantravahi, M. Kauffman, S. Shacham, A. Chenchik, K. Bonneau, K. S. Ullman, T. O'Hare, M.W. Deininger, shRNA library screening identifies nucleocytoplasmic transport as a mediator of BCR-ABL1 kinase-independent resistance, Blood 125 (2015) 1772–1781.

[13] J. Fredebohm, J. Wolf, J.D. Hoheisel, M. Boettcher, Depletion of RAD17 sensitizes pancreatic cancer cells to gemcitabine, J. Cell Sci. 126 (2013) 3380–3389.

[14] K. Schramm, M. Iskar, B. Statz, N. Jäger, D. Haag, M. Slabicki, S.M. Pfister, M. Zapatka, J. Gronych, D.T.W. Jones, P. Lichter, DECIPHER pooled shRNA library screen identifies PP2A and FGFR signaling as potential therapeutic targets for diffuse intrinsic pontine gliomas, Neuro Oncol. 21 (2019) 867–877.

[15] E. Yeger-Lotem, L. Riva, L.J. Su, A.D. Gitler, A.G. Cashikar, O.D. King, P.K. Auluck, M.L. Geddie, J.S. Valastyan, D.R. Karger, S. Lindquist, E. Fraenkel, Bridging high-throughput genetic and transcriptional data reveals cellular responses to alpha-synuclein toxicity, Nat. Genet. 41 (2009) 316–323.

[16] S.J. Gosline, S.J. Spencer, O. Ursu, E. Fraenkel, SAMNet: a network-based approach to integrate multi-dimensional high throughput datasets, Integr. Biol. 4 (2012) 1415–1427.

[17] R.J. Kinsella, A. Kähäri, S. Haider, J. Zamora, G. Proctor, G. Spudich, J. Almeida-King, D. Staines, P. Derwent, A. Kerhornou, P. Kersey, P. Flicek, Ensembl BioMarts: a hub for data retrieval across taxonomic space, Database 2011 (2011) bar030.

[18] K. Krug, P. Mertins, B. Zhang, P. Hornbeck, R. Raju, R. Ahmad, M. Szucs, F. Mundt, D. Forestier, J. Jane-Valbuena, H. Keshishian, M.A. Gillette, P. Tamayo, J. P. Mesirov, J.D. Jaffe, S.A. Carr, D.R. Mani, A curated resource for phosphosite-specific signature analysis, Mol. Cell. Proteomics 18 (2019) 576–593.

[19] Z. Dai, J.M. Sheridan, L.J. Gearing, D.L. Moore, S. Su, S. Wormald, S. Wilcox, L. O'Connor, R.A. Dickins, M.E. Blewitt, M.E. Ritchie, edgeR: a versatile tool for the analysis of shRNA-seq and CRISPR-Cas9 genetic screens, F1000Res 3 (2014) 95.

[20] D. Wu, G.K. Smyth, Camera: a competitive gene set test accounting for inter-gene correlation, Nucleic Acids Res. 40 (2012) e133.

[21] D. Hausmann, D.C. Hoffmann, V. Venkataramani, E. Jung, S. Horschitz, S. K. Tetzlaff, A. Jabali, L. Hai, T. Kessler, D.D. Azořin, S. Weil, A. Kourtesakis, P. Sievers, A. Habel, M.O. Breckwoldt, M.A. Karreman, M. Ratliff, J.M. Messmer, Y. Yang, E. Reyhan, S. Wendler, C. Löb, C. Mayer, K. Figarella, M. Osswald, G. Solecki, F. Sahm, O. Garaschuk, T. Kuner, P. Koch, M. Schlesner, W. Wick, F. Winkler, Autonomous rhythmic activity in glioma networks drives brain tumour growth, Nature 613 (2023) 179–186.

[22] L. Borghese, D. Dolezalova, T. Opitz, S. Haupt, A. Leinhaas, B. Steinfarz, P. Koch, F. Edenhofer, A. Hampl, O. Brüstle, Inhibition of notch signaling in human embryonic stem cell-derived neural stem cells delays G1/S phase transition and accelerates neuronal differentiation in vitro and in vivo, Stem Cell. 28 (2010) 955–964.

[23] S.M. Chambers, C.A. Fasano, E.P. Papapetrou, M. Tomishima, M. Sadelain, L. Studer, Highly efficient neural conversion of human ES and iPS cells by dual inhibition of SMAD signaling, Nat. Biotechnol. 27 (2009) 275–280.
[24] P.V. Hornbeck, B. Zhang, B. Murray, J.M. Kornhauser, V. Latham, E. Skrzypek, PhosphoSitePlus, 2014: mutations, PTMs and recalibrations, Nucleic Acids Res. 43 (2015) D512–D520.
[25] J.C. Obenauer, L.C. Cantley, M.B. Yaffe, Scansite 2.0: proteome-wide prediction of cell signaling interactions using short sequence motifs, Nucleic Acids Res. 31 (2003) 3635–3641.
[26] P. Kaldis, The cdk-activating kinase (CAK): from yeast to mammals, Cell. Mol. Life Sci. 55 (1999) 284–296.
[27] J.R. Burke, G.L. Hura, S.M. Rubin, Structures of inactive retinoblastoma protein reveal multiple mechanisms for cell cycle control, Gene Dev. 26 (2012) 1156–1166.
[28] A.M. Martinez, M. Afshar, F. Martin, J.C. Cavadore, J.C. Labbé, M. Dorée, Dual phosphorylation of the T-loop in cdk7: its role in controlling cyclin H binding and CAK activity, EMBO J. 16 (1997) 343–354.
[29] C.J. Matheson, D.S. Backos, P. Reigan, Targeting WEE1 kinase in cancer, Trends Pharmacol. Sci. 37 (2016) 872–881.
[30] C.M. Toledo, Y. Ding, P. Hoellerbauer, R.J. Davis, R. Basom, E.J. Girard, E. Lee, P. Corrin, T. Hart, H. Bolouri, J. Davison, Q. Zhang, J. Hardcastle, B.J. Aronow, C. L. Plaisier, N.S. Baliga, J. Moffat, Q. Lin, X.N. Li, D.H. Nam, J. Lee, S.M. Pollard, J. Zhu, J.J. Delrow, B.E. Clurman, J.M. Olson, P.J. Paddison, Genome-wide CRISPR-Cas9 screens reveal loss of redundancy between PKMYT1 and WEE1 in glioblastoma stem-like cells, Cell Rep. 13 (2015) 2425–2439.
[31] C.H. McGowan, P. Russell, Cell cycle regulation of human WEE1, EMBO J. 14 (1995) 2166–2175.
[32] E.J. Wojcik, R.S. Buckley, J. Richard, L. Liu, T.M. Huckaba, S. Kim, Kinesin-5: cross-bridging mechanism to targeted clinical therapy, Gene 531 (2013) 133–149.
[33] C.J. Rothblum-Oviatt, C.E. Ryan, H. Piwnica-Worms, 14-3-3 binding regulates catalytic activity of human Wee1 kinase, Cell Growth Differ. 12 (2001) 581–589.
[34] K. Okamoto, N. Sagata, Mechanism for inactivation of the mitotic inhibitory kinase Wee1 at M phase, Proc. Natl. Acad. Sci. U. S. A. 104 (2007) 3753–3758.
[35] C.W. Cheng, E. Tse, PIN1 in cell cycle control and cancer, Front. Pharmacol. 9 (2018) 1367.
[36] S.E. Mir, P.C. De Witt Hamer, P.M. Krawczyk, L. Balaj, A. Claes, J.M. Niers, A. A. Van Tilborg, A.H. Zwinderman, D. Geerts, G.J. Kaspers, W. Peter Vandertop, J. Cloos, B.A. Tannous, P. Wesseling, J.A. Aten, D.P. Noske, C.J. Van Noorden, T. Würdinger, In silico analysis of kinase expression identifies WEE1 as a gatekeeper against mitotic catastrophe in glioblastoma, Cancer Cell 18 (2010) 244–257.
[37] N. Tuncbag, P. Milani, J.L. Pokorny, H. Johnson, T.T. Sio, S. Dalin, D.O. Iyekegbe, F.M. White, J.N. Sarkaria, E. Fraenkel, Network modeling identifies patient-specific pathways in glioblastoma, Sci. Rep. 6 (2016) 28668.
[38] D.R. Kellogg, Wee1-dependent mechanisms required for coordination of cell growth and cell division, J. Cell Sci. 116 (2003) 4883–4890.
[39] D. Music, R.H. Dahlrot, S.K. Hermansen, J. Hjelmborg, K. de Stricker, S. Hansen, B. W. Kristensen, Expression and prognostic value of the WEE1 kinase in gliomas, J. Neuro Oncol. 127 (2016) 381–389.
[40] H. Hochegger, S. Takeda, T. Hunt, Cyclin-dependent kinases and cell-cycle transitions: does one fit all? Nat. Rev. Mol. Cell Biol. 9 (2008) 910–916.
[41] D. Parry, T. Guzi, F. Shanahan, N. Davis, D. Prabhavalkar, D. Wiswell, W. Seghezzi, K. Paruch, M.P. Dwyer, R. Doll, A. Nomeir, W. Windsor, T. Fischmann, Y. Wang, M. Oft, T. Chen, P. Kirschmeier, E.M. Lees, Dinaciclib (SCH 727965), a novel and potent cyclin-dependent kinase inhibitor, Mol. Cancer Therapeut. 9 (2010) 2344–2353.
[42] Y. Zhou, L. Yang, X. Zhang, R. Chen, X. Chen, W. Tang, M. Zhang, Identification of potential biomarkers in glioblastoma through bioinformatic analysis and evaluating their prognostic value, BioMed Res. Int. 2019 (2019) 6581576.
[43] W. Wei, Y.S. Shin, M. Xue, T. Matsutani, K. Masui, H. Yang, S. Ikegami, Y. Gu, K. Herrmann, D. Johnson, X. Ding, K. Hwang, J. Kim, J. Zhou, Y. Su, X. Li, B. Bonetti, R. Chopra, C.D. James, W.K. Cavenee, T.F. Cloughesy, P.S. Mischel, J. R. Heath, B. Gini, Single-cell phosphoproteomics resolves adaptive signaling dynamics and informs targeted combination therapy in glioblastoma, Cancer Cell 29 (2016) 563–573.
[44] R.S. Lescarbeau, L. Lei, K.K. Bakken, P.A. Sims, J.N. Sarkaria, P. Canoll, F. M. White, Quantitative phosphoproteomics reveals Wee1 kinase as a therapeutic target in a model of proneural glioblastoma, Mol. Cancer Therapeut. 15 (2016) 1332–1343.
[45] C.J. Wu, D.M. O'Rourke, G.S. Feng, G.R. Johnson, Q. Wang, M.I. Greene, The tyrosine phosphatase SHP-2 is required for mediating phosphatidylinositol 3-kinase/Akt activation by growth factors, Oncogene 20 (2001) 6018–6025.
[46] P.C. De Witt Hamer, S.E. Mir, D. Noske, C.J. Van Noorden, T. Würdinger, WEE1 kinase targeting combined with DNA-damaging cancer therapy catalyzes mitotic catastrophe, Clin. Cancer Res. 17 (2011) 4200–4207.
[47] S. Peng, B. Sen, T. Mazumdar, L.A. Byers, L. Diao, J. Wang, P. Tong, U. Giri, J. V. Heymach, H.N. Kadara, F.M. Johnson, Dasatinib induces DNA damage and activates DNA repair pathways leading to senescence in non-small cell lung cancer cell lines with kinase-inactivating BRAF mutations, Oncotarget 7 (2016) 565–579.
[48] M. Cozzi, F. Giorgi, E. Marcelli, F. Pentimalli, I.M. Forte, S. Schenone, V. D'Urso, G. De Falco, M. Botta, A. Giordano, P. Indovina, Antitumor activity of new pyrazolo [3,4-d]pyrimidine SRC kinase inhibitors in Burkitt lymphoma cell lines and its enhancement by WEE1 inhibition, Cell Cycle 11 (2012) 1029–1039.
[49] Y. Oku, N. Nishiya, T. Tazawa, T. Kobayashi, N. Umezawa, Y. Sugawara, Y. Uehara, Augmentation of the therapeutic efficacy of WEE1 kinase inhibitor AZD1775 by inhibiting the YAP-E2F1-DNA damage response pathway axis, FEBS Open Bio 8 (2018) 1001–1012.
[50] L.A. Gravendeel, M.C. Kouwenhoven, O. Gevaert, J.J. de Rooi, A.P. Stubbs, J. E. Duijm, A. Daemen, F.E. Bleeker, L.B. Bralten, N.K. Kloosterhof, B. De Moor, P. H. Eilers, P.J. van der Spek, J.M. Kros, P.A. Sillevis Smitt, M.J. van den Bent, P. J. French, Intrinsic gene expression profiles of gliomas are a better predictor of survival than histology, Cancer Res. 69 (2009) 9065–9072.